INTERNATIONAL JOURNAL FOR NUMERICAL AND ANALYTICAL METHODS IN GEOMECHANICS
Int. J. Numer. Anal. Meth. Geomech., **23,** 779–800 (1999)

SOLUTIONS FOR THE DEFORMATIONS AND STABILITY OF ELASTOPLASTIC HOLLOW CYLINDERS SUBJECTED TO BOUNDARY PRESSURES

X. CHEN[1,2,*], C. P. TAN[1] AND C. M. HABERFIELD[2]

[1] *Australian Petroleum Cooperative Research Centre, CSIRO Petroleum, Glen Waverley, Victoria 3150, Australia*
[2] *Department of Civil Engineering, Faculty of Engineering, Monash University, Claytion, Victoria 3168, Australia*

SUMMARY

In this paper, a closed-form solution is presented for the stress and displacement distributions throughout a hollow cylinder subjected to uniform pressures acting on its internal and external boundary surfaces under plane strain conditions. The material is assumed to be elastoplastic, obeying a Mohr–Coulomb failure criterion, and exhibiting dilatant plastic deformation according to a non-associated flow rule. The newly developed analytical solution is verified through comparison with the solutions obtained from an infinite boundary problem (for which a closed-form solution exists), and numerical analyses using the program FLAC. The solution is also compared with the results of a borehole collapse test on a thick-walled hollow cylinder of synthetic shale.

The analytical solution can be used to calculate the stress and displacement distributions around boreholes and other cylindrical cavities under both infinite and finite boundary conditions under both drained and undrained conditions.

Key words: hollow cylinder; borehole stability; analytical solution

1. INTRODUCTION

The stability of boreholes and large-sized cylindrical cavities in an infinite medium is of significant interest in the petroleum, mining and geotechnical industries. The analysis of an internally pressurized borehole is essential not only in reducing unnecessary high costs of drilling and excavation but also for interpreting pressuremeter and penetrometer tests and pile-driving phenomena in geotechnical engineering. In order to better quantify the phenomena and to refine the accuracy of existing models, a better understanding of the mechanical properties and deformation behaviour of rocks is essential. As small-scale modelling of geotechnical problems is a relatively inexpensive and convenient way of studying prototype behaviour and offers valuable insights into the likely prototype response, a borehole collapse test on thick-walled hollow cylindrical sample can be conducted to improve our understanding of borehore deformation behaviour.

* Correspondence to: X. Chen, CSIRO Petroleum, PO Box 3000, Glen Waverley, Vic 3150, Australia

CCC 0363–9061/99/080779–22$17.50

Received 29 January 1998
Revised 31 August 1998

It is logical and desirable to compare the test results with analytical predictions. However, the various analytical and semi-analytical solutions which have been developed have concentrated on infinite boundary problems.[1–8] Most of these solutions are based on elastic/perfectly plastic models and restricted to Mohr–Coulomb or Tresca materials. Due to the complexity of the finite boundary problem, no complete analytical solution for stress and displacement prediction for Mohr–Coulomb materials appears to have been presented so far, although similar work has been conducted previously.[9–14] It is necessary, therefore, to develop an equivalent analytical solution for the prediction of stress and displacement distributions of laboratory borehole collapse tests on thick-walled hollow cylinders.

In this paper, a closed-form solution is presented for the stress and displacement distributions throughout a hollow cylinder subjected to uniform pressures acting on its internal and external boundary surfaces under plane strain conditions. The material is assumed to be elastoplastic, obeying a Mohr–Coulomb failure criterion, and exhibiting dilatant plastic deformation according to a non-associated flow rule. The newly developed analytical solution is verified through comparison with the solutions obtained from an infinite boundary problem (for which a closed-form solution exists), and numerical analyses using the program FLAC.[15] The solution is also compared with the results of a borehole collapse test on a thick-walled hollow cylinder of synthetic shale.

2. DERIVATION OF THE CLOSED-FORM SOLUTION

2.1. Assumptions and basic equations

To enable a solution to be determined, the following assumptions are necessary:

(1) The hollow cylinder is infinitely long, and is subjected to a pressure, P_o, over its entire outer surface and a pressure, P_i, over its entire internal surface. Hence, conditions of plane strain and axisymmetry are appropriate.
(2) Effective stresses and strengths are adopted.
(3) The material is homogeneous and isotropic.
(4) The material is linear elastic up to yield which is determined from the Mohr–Coulomb failure criterion:

$$\sigma_1 = m\sigma_3 + \frac{2c\cos\phi}{1-\sin\phi} \tag{1}$$

where σ_1, σ_3 are the maximum and minimum principal stresses, respectively, c is cohesion, ϕ is friction angle, and

$$m = \frac{1+\sin\phi}{1-\sin\phi} \tag{2}$$

While the material is elastic, stresses and strains are related by Hooke's law, i.e.

$$\begin{Bmatrix}\varepsilon_1\\ \varepsilon_2\\ \varepsilon_3\end{Bmatrix} = \frac{1}{E}\begin{bmatrix}1 & -v & -v\\ -v & 1 & -v\\ -v & -v & 1\end{bmatrix}\begin{Bmatrix}\sigma_1\\ \sigma_2\\ \sigma_3\end{Bmatrix} \tag{3}$$

where ε_1, ε_2, ε_3 are the principal strains, σ_1, σ_2, σ_3 are the principal stresses, E is Young's modulus, and v is Poisson's ratio. The plane strain assumption results in $\varepsilon_2 = 0$.

(5) At failure, the material behaves according to the linear Mohr–Coulomb failure criterion as given in equation (1).

(6) Once the material has yielded, stresses can no longer be evaluated directly from strains but must be determined by the yield criterion. The incremental strains at yield can be obtained by determining the values of the elastic and plastic components, i.e.

$$d\varepsilon = d\varepsilon^e + d\varepsilon^p \tag{4}$$

The elastic component is determined by Hooke's law while the plastic component is determined by a flow rule. A non-associative flow rule which expresses the amount of plastic volume change of the material in terms of dilation angle, ψ, has been adopted.[16] This flow rule can be expressed in terms of principal plastic strain increments as

$$\begin{Bmatrix} d\varepsilon_1^p \\ d\varepsilon_2^p \\ d\varepsilon_3^p \end{Bmatrix} = d\lambda \begin{Bmatrix} -n \\ 0 \\ 1 \end{Bmatrix} \tag{5}$$

where $d\lambda$ is a plastic multiplier, and

$$n = \frac{1 + \sin\psi}{1 - \sin\psi} \tag{6}$$

(7) Strains remain small and hence, small deflection theory is applicable.

(8) Compressive stresses are assumed to be positive.

The solution to this problem is best achieved by adopting a cylindrical co-ordinate system. The problem can thus be described by Figure 1. As this is an axisymmetric problem, the strain displacement and equilibrium equations of elasticity theory can be reduced to the following form:

Strain displacement equation:

$$\begin{Bmatrix} \varepsilon_r \\ \varepsilon_\theta \end{Bmatrix} = \begin{Bmatrix} \dfrac{du_r}{dr} \\ \dfrac{u_r}{r} \end{Bmatrix} \tag{7}$$

Equilibrium equation:

$$\frac{d\sigma_r}{dr} + \frac{\sigma_r - \sigma_\theta}{r} = 0 \tag{8}$$

where σ_r, σ_θ are the radial and circumferential stresses, ε_r, ε_θ are the radial and circumferential strains, and u_r is the radial displacement at radius r.

2.2. Stress distribution in the plastic zone

If the yield strength of the material is reached, a circular plastic zone develops around the internal boundary of the cylinder. In Figure 1, r_f is the radius of the boundary between the plastic and elastic zones. In the plastic zone ($a \leqslant r \leqslant r_f$), the stress distribution is obtained by combining

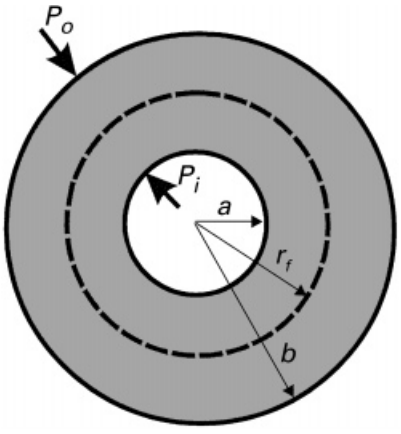

Figure 1. Problem geometry under plane strain conditions

the failure criterion (the Mohr–Coulomb criterion as given in equation (1)) with the equilibrium equation (equation (8)). Although the solution presented is exact[3] for $(m+1)v \geqslant 1$, for most borehole breakout problems, $\sigma_1 = \sigma_\theta$, $\sigma_3 = \sigma_r$ and $\sigma_2 = \sigma_z$.[17] Substituting equation (1) into equation (8) gives

$$r\frac{\mathrm{d}\sigma_{rp}}{\mathrm{d}r} + \sigma_{rp} - m\sigma_{rp} - \frac{2c\cos\phi}{1-\sin\phi} = 0 \tag{10}$$

where σ_{rp} is the radial stress in the plastic zone at radius r.

Rearranging the above:

$$\frac{\mathrm{d}\sigma_{rp}}{\sigma_{rp} + c\cot\phi} = \frac{2\sin\phi}{1-\sin\phi}\frac{\mathrm{d}r}{r} \tag{11}$$

Integrating equation (11) gives

$$\sigma_{rp} + c\cot\phi = Ar^q \tag{12}$$

where

$$q = \frac{2\sin\phi}{1-\sin\phi} \tag{13}$$

As $\sigma_{rp} = P_\mathrm{i}$ at $r = a$, the above equation becomes

$$A = \frac{P_\mathrm{i} + c\cot\phi}{a^q} \tag{14}$$

Substituting equation (14) into equation (12) enables the radial stress at a radius r to be obtained. By substituting the radial stress into the Mohr–Coulomb failure criterion (equation (1)), the

circumferential stress can also be determined. The solutions are given below:

$$\sigma_{r\mathrm{p}} = c \cot\phi \left[\left(\frac{r}{a} \right)^q - 1 \right] + P_\mathrm{i} \left(\frac{r}{a} \right)^q \tag{15}$$

$$\sigma_{\theta\mathrm{p}} = c \cot\phi \left[m \left(\frac{r}{a} \right)^q - 1 \right] + m P_\mathrm{i} \left(\frac{r}{a} \right)^q \tag{16}$$

Hence, the radial stress, P_f, at the boundary of plastic and elastic zones at radius r_f can be derived from equation (15):

$$P_\mathrm{f} = c \cot\phi \left[\left(\frac{r_\mathrm{f}}{a} \right)^q - 1 \right] + P_\mathrm{i} \left(\frac{r_f}{a} \right)^q \tag{17}$$

2.3. Stress distribution in the elastic zone

The elastic stress distribution for a hollow cylinder can be derived by combining Hooke's law (equation (3)) with the equilibrium equation (equation (8)). The stress distribution in the elastic zone is determined by considering the hollow cylinder of internal radius, r_f, with an internal pressure, P_f, and external radius, b, with an external pressure, P_o. Since the solution has been given in many publications, e.g. Reference 18, the derivation details are not presented here. Only the final equations are given below:

$$\sigma_r = \frac{b^2 r_\mathrm{f}^2 (P_\mathrm{f} - P_\mathrm{o})}{b^2 - r_\mathrm{f}^2} \times \frac{1}{r^2} + \frac{b^2 P_0 - r_\mathrm{f}^2 P_\mathrm{f}}{b^2 - r_\mathrm{f}^2} \tag{18}$$

$$\sigma_\theta = -\frac{b^2 r_\mathrm{f}^2 (P_\mathrm{f} - P_\mathrm{o})}{b^2 - r_\mathrm{f}^2} \times \frac{1}{r^2} + \frac{b^2 P_0 - r_\mathrm{f}^2 P_\mathrm{f}}{b^2 - r_\mathrm{f}^2} \tag{19}$$

$$\sigma_z = \frac{1}{2} (\sigma_r + \sigma_\theta) = \frac{b^2 P_0 - r_\mathrm{f}^2 P_\mathrm{f}}{b^2 - r_\mathrm{f}^2} \tag{20}$$

2.4. Outer radius of the plastic zone

From equilibrium, the radial stress at the boundary between plastic and elastic zones ($r = r_\mathrm{f}$) is equal, i.e.

$$\sigma_r = \sigma_{r\mathrm{p}} \tag{21}$$

and hence to satisfy the failure criterion

$$\sigma_\theta = \sigma_{\theta\mathrm{p}} \tag{22}$$

Substituting equations (16) and (19) into equation (22) and after rearranging, the following equation is obtained:

$$[b^2(m+1) - r_\mathrm{f}^2(m-1)](c \cot\phi + P_\mathrm{i}) \left(\frac{r_\mathrm{f}}{a} \right)^q = 2b^2 (P_\mathrm{o} + c \cot\phi) \tag{23}$$

At the initiation of yield, the material at the internal wall of a hollow cylinder has just yielded and hence $r_f = a$. Substituting into equation (23) gives

$$P_i(b^2 - a^2 \sin\phi) - P_o b^2(1 - \sin\phi) = c\cos\phi(a^2 - b^2) \tag{24}$$

When the entire hollow cylinder has yielded, $r_f = b$ and substituting this value for the radius into equation (23) gives

$$P_o - P_i\left(\frac{b}{a}\right)^q = c\cot\phi\left[\left(\frac{b}{a}\right)^q - 1\right] \tag{25}$$

2.5. Displacement distribution in the plastic zone

The elastic components of total strain, obtained by substituting equations (15) and (16) into equation (3), are given below:

$$\varepsilon_r^e = \frac{1}{E}\left[(2v^2 + v - 1)c\cot\phi + (1 - v - vm - vm^2)(P_i + c\cot\phi)\left(\frac{r}{a}\right)^q\right] \tag{26}$$

$$\varepsilon_\theta^e = \frac{1}{E}\left[(2v^2 + v - 1)c\cot\phi + (m - v - v^2m - v^2)(P_i + c\cot\phi)\left(\frac{r}{a}\right)^q\right] \tag{27}$$

From equation (5), the following equation relating incremental plastic strains can be obtained:

$$\mathrm{d}\varepsilon_r^p + n\,\mathrm{d}\varepsilon_\theta^p = 0 \tag{28}$$

Integrating the equation gives

$$\varepsilon_r^p + n\varepsilon_\theta^p = A \text{ (constant)} \tag{29}$$

The constant A in equation (29) can be determined by the boundary conditions at $r = r_f$ given below and the constant is found to be equal to zero:

$$\begin{aligned}\Delta\varepsilon_{r+}^e &= \Delta\varepsilon_{r-}^e + \Delta\varepsilon_r^p\\ \Delta\varepsilon_{\theta+}^e &= \Delta\varepsilon_{\theta-}^e + \Delta\varepsilon_\theta^p\end{aligned} \tag{30}$$

where the subscript ' + ' refers to the value at $r = r_f$ assuming elastic behaviour, and ' − ' refers to the value at $r = r_f$ assuming plastic behaviour.

Rearranging the strain displacement relationship (equation (7)) gives

$$\varepsilon_r = \varepsilon_\theta + r\frac{\mathrm{d}\varepsilon_\theta}{\mathrm{d}r} \tag{31}$$

Combining equations (4) and (31) gives

$$r\frac{\mathrm{d}\varepsilon_\theta^p}{\mathrm{d}r} + (n+1)\varepsilon_\theta^p = \varepsilon_r^e - \varepsilon_\theta^e - r\frac{\mathrm{d}\varepsilon_\theta^e}{\mathrm{d}r} \tag{32}$$

where ε_r^e, ε_θ^e and $\mathrm{d}\varepsilon_\theta^e/\mathrm{d}r$ can be evaluated from equations (26) and (27).

Solving equation (32) gives

$$\varepsilon_\theta^p = \frac{1}{r^{n+1}}\left[B + \frac{r^{n+1}(r/a)^q(1+v)(1-m-qm+mqv+qv)(c\cot\phi + P_i)}{E(1+n+q)}\right] \tag{33}$$

where B is the constant which can be determined by applying the boundary conditions given in equation (30). Hence $\varepsilon_\theta^{\mathrm{p}}$ can be obtained as given below:

$$\varepsilon_\theta^{\mathrm{p}} = \frac{(1+v)(1-m-qm+mqv+qv)(c\cot\phi + P_{\mathrm{i}})}{E(1+n+q)} \frac{1}{r^{n+1}} \left[r^{n+1}(r/a)^q - r_{\mathrm{f}}^{n+1}(r_{\mathrm{f}}/a)^q \right] \tag{34}$$

The total circumferential strain can be obtained by adding equations (27) and (34), and the total radial displacement is obtained as given below:

$$u_r = \frac{(1+v)r}{E} \left[k_1 + k_2(k_3+k_4)\left(\frac{r}{a}\right)^q - k_2 k_4 \left(\frac{r_{\mathrm{f}}}{a}\right)^q \left(\frac{r_{\mathrm{f}}}{r}\right)^{n+1} \right] \tag{35}$$

where

$$\begin{aligned} k_1 &= (2v-1)c\cot\phi \\ k_2 &= P_{\mathrm{i}} + c\cot\phi \\ k_3 &= m - mv - v \\ k_4 &= \frac{1-m-mq+mqv+qv}{1+n+q} \end{aligned} \tag{36}$$

2.6. Displacement distribution in the elastic zone

The circumferential strain in the elastic zone is obtained by substituting equation (19) into equation (3):

$$\varepsilon_\theta = \frac{1-v-2v^2}{E} \frac{b^2P_{\mathrm{o}} - r_{\mathrm{f}}^2P_{\mathrm{f}}}{b^2 - r_{\mathrm{f}}^2} + \frac{1+v}{E} \frac{b^2r_{\mathrm{f}}^2(P_{\mathrm{o}} - P_{\mathrm{f}})}{b^2 - r_{\mathrm{f}}^2} \frac{1}{r^2} \tag{37}$$

The radial displacement is obtained from equation (7):

$$u_r = \frac{1-v-2v^2}{E} \frac{b^2P_{\mathrm{o}} - r_{\mathrm{f}}^2P_{\mathrm{f}}}{b^2 - r_{\mathrm{f}}^2} r + \frac{1+v}{E} \frac{b^2r_{\mathrm{f}}^2(P_{\mathrm{o}} - P_{\mathrm{f}})}{b^2 - r_{\mathrm{f}}^2} \frac{1}{r} \tag{38}$$

3. VALIDATION OF THE CLOSED-FORM SOLUTION

3.1. Comparison with Fritz's solution

Fritz[4] developed an analytical solution for axisymmetric tunnel problems in elasto-viscoplastic media. The theoretical assumptions and derivation procedures of Fritz's solution are similar to those for the newly developed solution presented in Section 2 but Fritz's solution is only applicable for infinite boundary problems. Since the two analytical solutions are based on similar assumptions, the new solution should reduce to Fritz's solution for an elastoplastic material with an outer radius approaching infinity. For simplicity, the similarity between the two solutions is demonstrated below for one set of parameters only. The material properties and geometry used in the comparison are given in Table I (refer to Figure 1). The new solution is converted to infinite boundary conditions by having an outer radius, b, of 5000 mm ($b/a \approx 400$).

Figure 2 compares the stress and radial displacement distributions with radius as obtained from Fritz's infinite boundary solution and from the newly derived finite boundary solution. It

Table I. Material properties and geometry parameters

a (mm)	b (mm)	c (MPa)	ϕ (deg)	ψ (deg)	E (MPa)	v	P_o (MPa)	P_i (MPa)	P_w (MPa)
12·8	5000	6·3	36·2	0	6·1	0·25	68	68 to 6	5

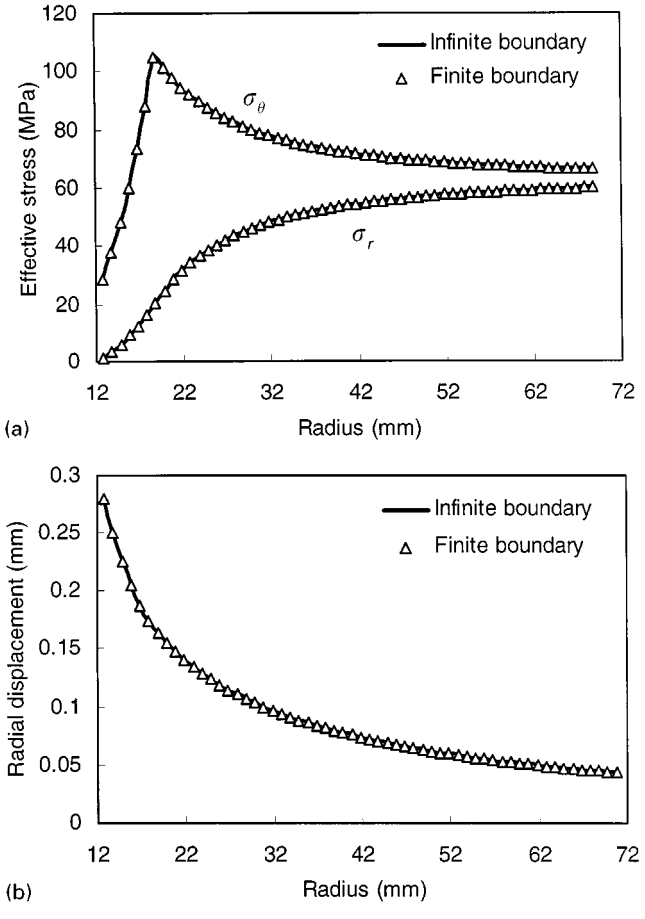

Figure 2. Comparison of infinite and finite boundary solutions. (a) Stress distribution along the radius; (b) displacement distribution along the radius

can be seen that when the outer radius, b, is significantly greater than the borehole radius, a, both solutions give essentially the same results. In addition, it was found that significantly different results are only obtained when the ratio of outer radius to inner radius, b/a, is less than about 14. The stress distribution given in Figure 2(a) suggests that a circular zone of 18·84 mm radius has yielded under the prescribed loading conditions.

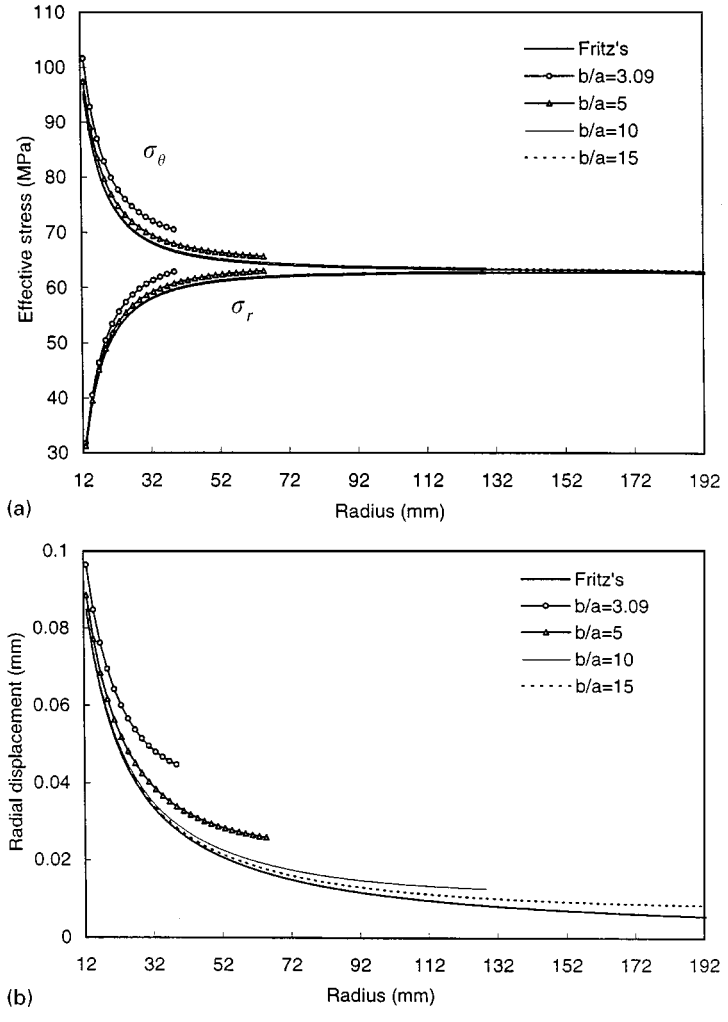

Figure 3. Comparison of infinite and finite boundary solutions at P_o of 68 MPa and P_i of 40 MPa (no yield). (a) stress distribution along the radius; (b) displacement distribution along the radius

Due to the absence of a solution for finite boundary problems, many laboratory experiments on hollow cylinders have been interpreted using Fritz's solution. Such interpretations have been carried out without any knowledge of error arising from the infinite boundary assumption. The percentage error can be investigated by comparing the results obtained with the newly derived and Fritz's solutions for various values of b/a over a range of internal pressures. Three example results, which represent no yield ($P_i = 40$ MPa), just yielded ($P_i = 25$ MPa) and extensively yielded ($P_i = 6$ MPa), are illustrated in Figures 3, 4 and 5, respectively. Their corresponding percentage errors are summarized in Figures 6–8.

It can be seen that the more extensive the material yielded, the larger is the percentage error. The percentage error increases with radial distance from the centre of the borehole and with decreasing ratios of b/a.

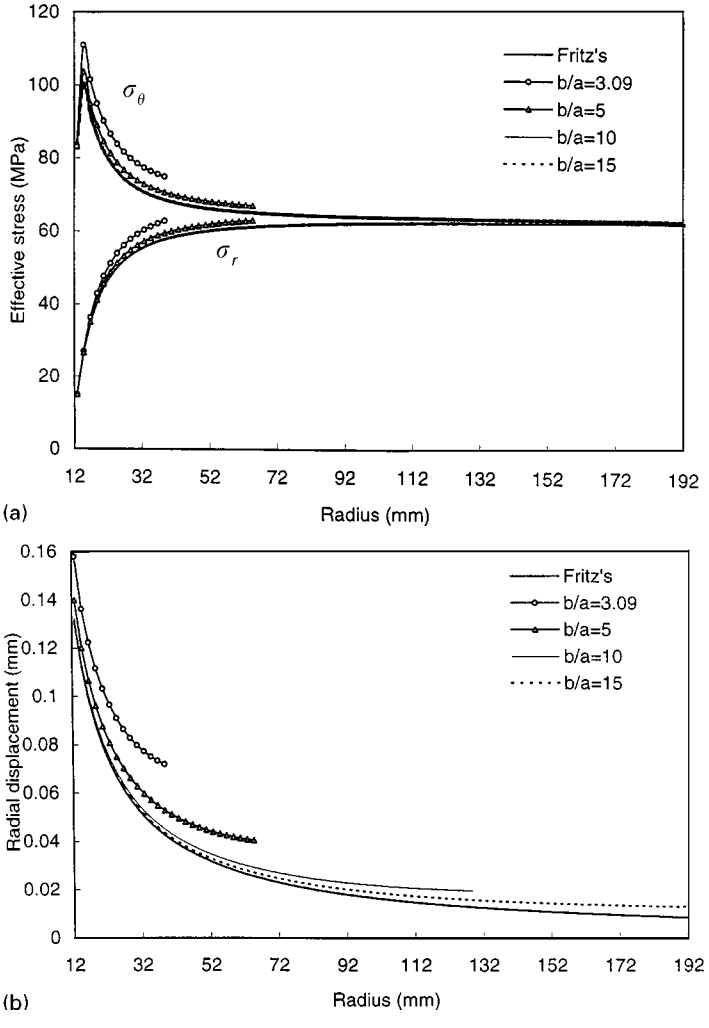

Figure 4. Comparison of infinite and finite boundary solutions at P_o of 68 MPa and P_i of 20 MPa (just yielded). (a) stress distribution along the radius; (b) displacement distribution along the radius

The investigation shows that an infinite boundary solution is a reasonable approximation if stresses are of concern, especially when the material has not yielded significantly (percentage error < 10 per cent). However, when determining stresses in material undergoing significant yield and/or accurate determination of displacement is important, the infinite boundary solution will lead to significant error (> 10 per cent).

3.2. Comparison with numerical model

The newly developed analytical solution is further applied to determine the borehole pressures which will result in initial and complete yielding of a thick-walled hollow cylinder which has

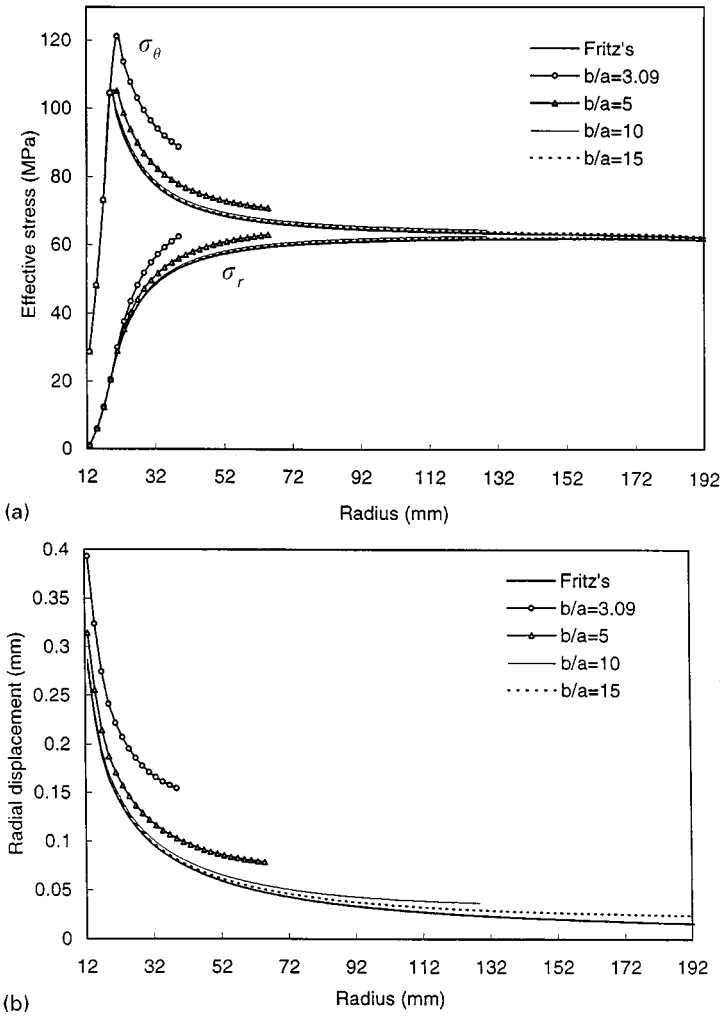

Figure 5. Comparison of infinite and finite boundary solutions at P_o of 68 MPa and P_i of 6 MPa (extensively yielded). (a) stress distribution along the radius; (b) displacement distribution along the radius

external diameter of 80 mm and internal diameter of 25 mm. In order to verify the analytical solution for finite boundary conditions, numerical modelling of the same problem has also been conducted and the comparison between the analytical and numerical results is presented and discussed.

The two-dimensional explicit finite difference program FLAC[15] was used to predict the deformation behaviour of the thick-walled hollow cylinder subjected to a constant external pressure, P_o, and a variable borehole pressure, P_i. A schematic of the plane strain numerical model is shown in Figure 9. The material properties used in the analysis are given in Table I.

Figures 10 and 11 present the borehole deformation and radius of yield zone versus borehole pressure, respectively. It can be seen from the figures that results obtained from the analytical

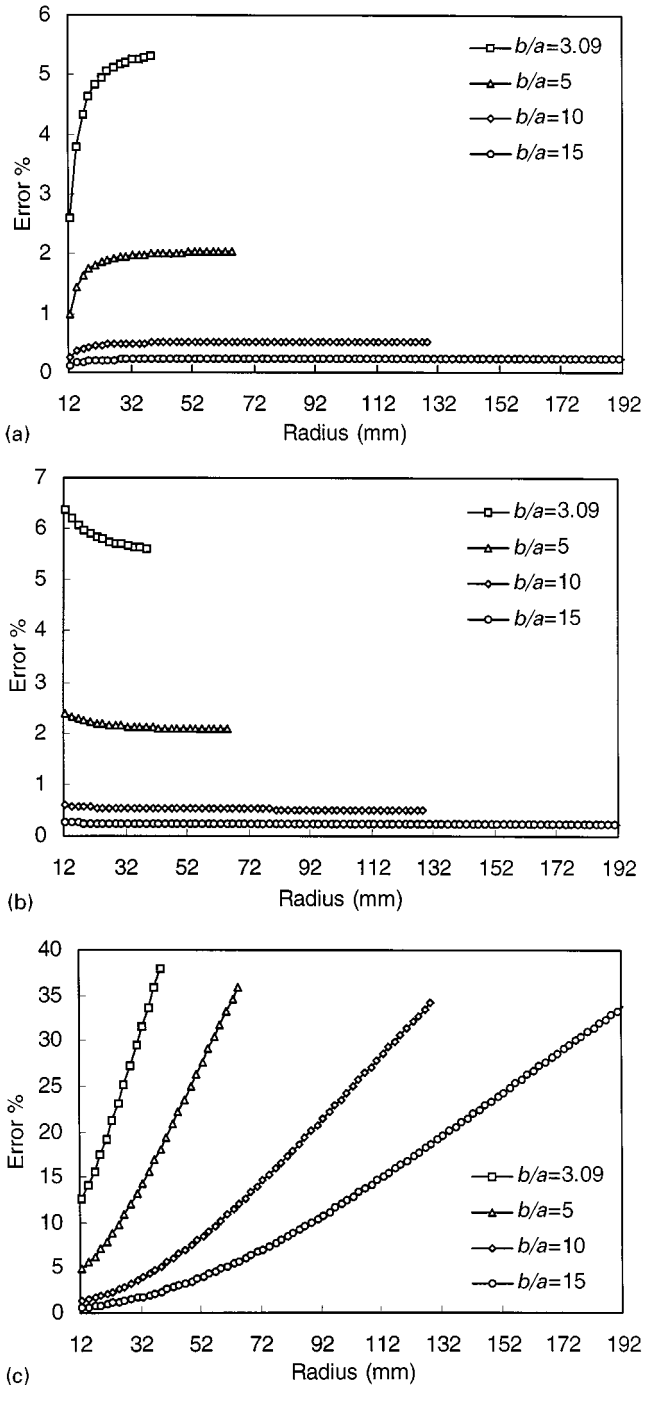

Figure 6. Percentage error at P_o of 68 MPa and P_i of 40 MPa (no yield). (a) radial stress σ_r; (b) circumferential stress σ_θ; (c) radial displacement u_r

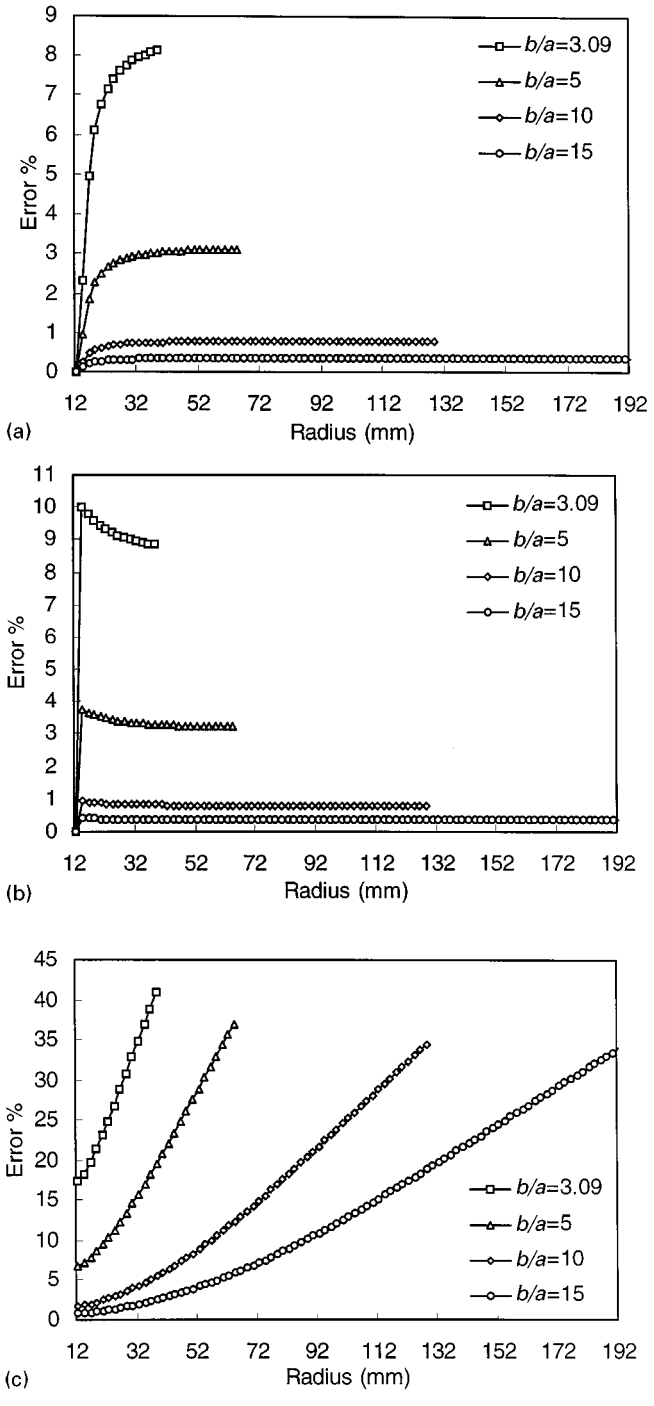

Figure 7. Percentage error at P_o of 68 MPa and P_i of 20 MPa (just yielded). (a) radialstress σ_r; (b) circumferential stress σ_θ; (c) radial displaceement u_r

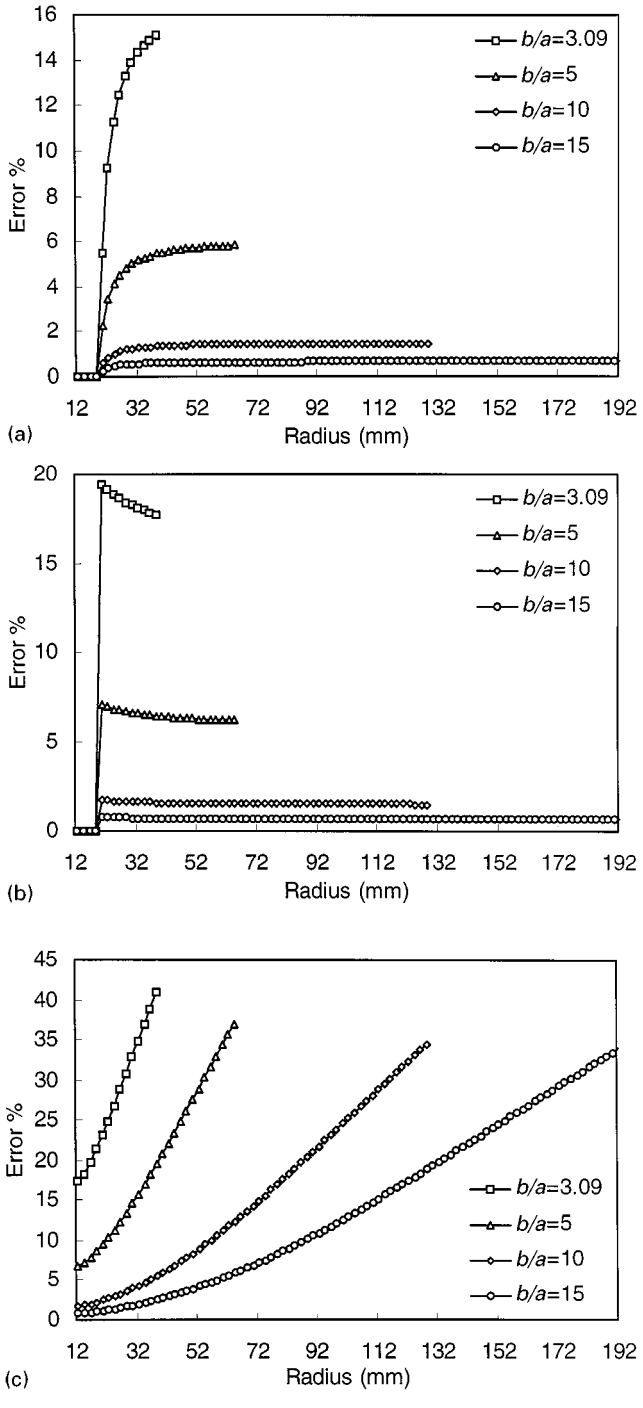

Figure 8. Percentage error at P_o of 68 MPa and P_i of 6 MPa (extensively yielded). (a) radial stress σ_r; (b) circumferential stress σ_θ; (c) radial displacement u_r

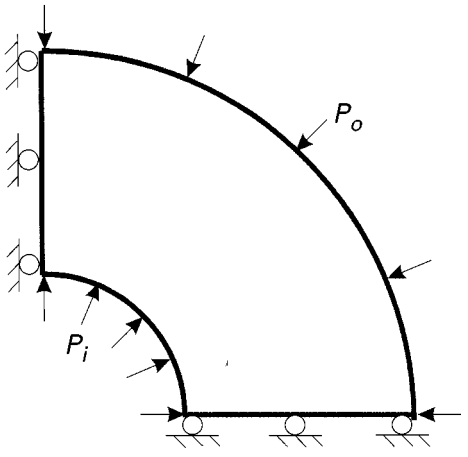

Figure 9. Conceptual model and boundary conditions

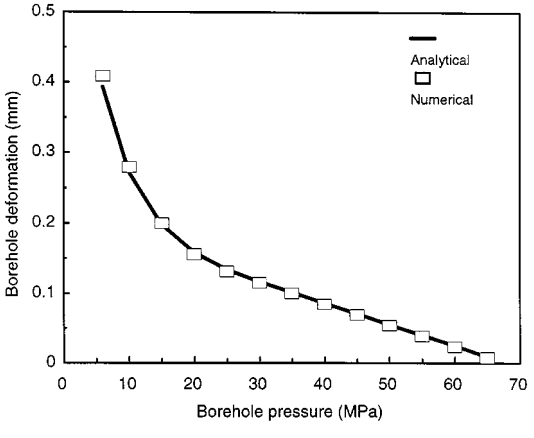

Figure 10. Borehole deformation versus borehole pressure

solution and numerical model are in good agreement. It is found that a borehole pressure of 27 MPa results in the initiation of yield.

Figure 12 shows the comparison of analytical and numerical stress and displacement distributions with radius at P_o of 68 MPa and P_i of 6 MPa. It can be seen that the solutions from the two methods agree well with each other. Both solutions show that a plastic zone of 19·93 mm radius has developed under the prescribed loading conditions. The radius of yield zone implies that complete yielding of the hollow cylinder has not occurred for a borehole pressure of 6 MPa (which is the minimum value of borehole pressure in the laboratory test presented in Section 4) under a confining pressure of 68 MPa. Moreover, the complete failure of the borehole will not occur for the worst case of a confining pressure of 68 MPa and a borehole pressure of 0 MPa, in which a circular yield zone of radius 30·86 mm has formed (of outer radius of 39·6 mm). To bring

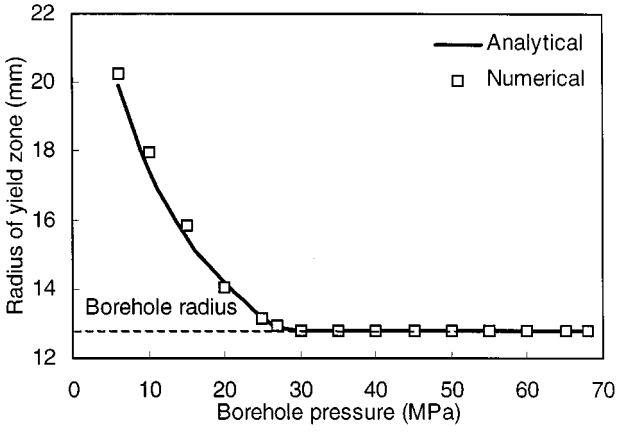

Figure 11. Radius of yield zone versus borehole pressure

about complete collapse of the borehole, the confining pressure needs to be 90 MPa for a borehole pressure of 0 MPa.

3.3. *Influence of dilation on displacement*

The results presented in the previous sections assumed a dilation angle $\psi = 0$. It may be of interest to briefly look at the effect of non-associativity on the results.

Figure 13 shows the radial displacement with radius for various values of dilation angle (represented by n defined in equation (6)) and assuming $P_o = 68$ MPa and $P_i = 6$ MPa. It can be seen that the difference at the borehole wall is very significant. For the example, up to 150 per cent difference in borehole displacement is obtained between $\psi = \phi$ and 0.

The difference in the borehole deformation also varies with internal pressures (i.e. extent of yield) as shown in Figure 14. For a relatively small yield zone, the difference is quite small, but increases dramatically as the radius of the yield zone increases.

The large influence of dilation angle on deformation indicates that a realistic dilation angle should be used for problems and applications where accurate deformation prediction is critical, such as in cavity excavation. However, it is less important for wellbore stability since stability is the major concern rather than borehole displacement.

4. APPLICATION OF THE SOLUTION TO BOREHOLE COLLAPSE TEST

The above analyses have verified the validity of the newly developed analytical solution. However, the ultimate purpose of the analytical solution is to predict the stress distribution and deformation behaviour, and corresponding wellbore (in)stability in laboratory simulations and/or field applications. It is necessary, therefore, to determine whether the analytical solution can predict the behaviour of laboratory tests on thick-walled cylinders of shale.

A borehole collapse test on a thick-walled hollow cylinder of a synthetic shale, modified Johnstone[19] was used for the comparison study. The test was carried out under undrained conditions, but with pore pressure measurement at the top and bottom of the sample. The test

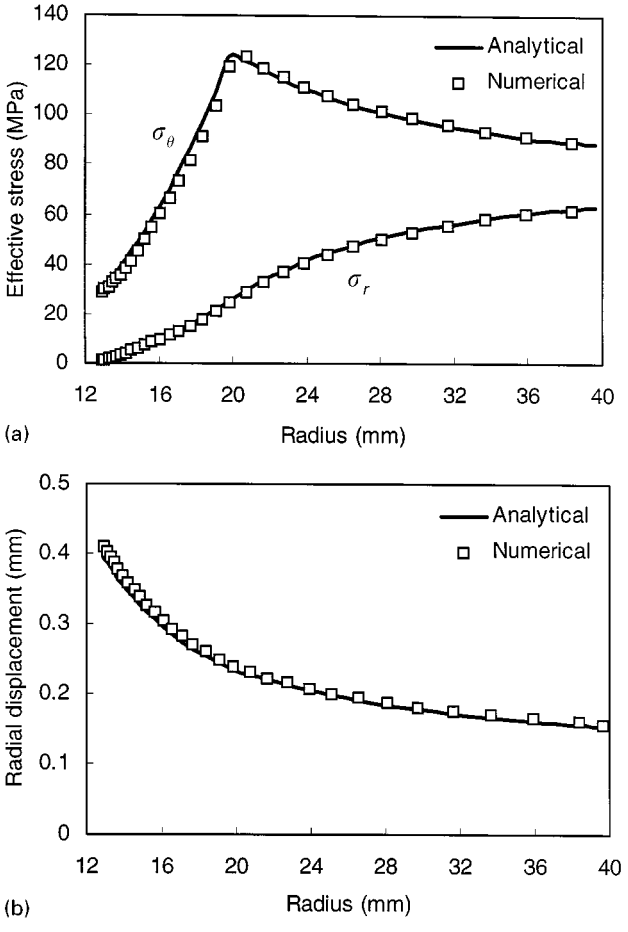

Figure 12. Comparison of stress and displacement distributions along radius at P_o of 68 MPa and P_i of 6 MPa. (a) stress distribution along radius; (b) displacement distribution along radius

was interpreted in terms of effective stresses. The sample has an outer diameter of 80 mm, inner diameter of 25 mm and a length of 160 mm. The test was conducted by decreasing borehole pressure, P_i, from its initial value of 68 to 6 MPa at a rate of 0·3 MPa/min while keeping external pressure, P_o, constant. This rate was selected based on the following considerations:

(a) Theoretically, the pore pressure distribution inside a homogeneous poroelastic hollow cylinder without end effects depends only on the magnitude of borehole pressure, not on the rate of borehole pressure reduction. The pore pressure is uniform inside the sample, i.e. there is no pore pressure gradient inside the sample.
(b) After initiation of yield and failure around the borehole, a decrease in pore pressure in the yield/failure zone is expected due to material dilation associated with plastic deformation. Equilibrium of pore pressure within the sample is extremely difficult to achieve due to the low permeability of the shale.

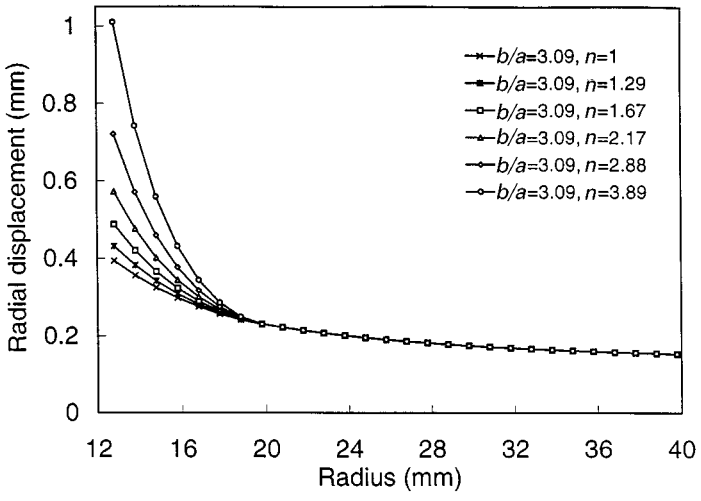

Figure 13. Comparison of radial displacement distribution under various non-associativity along radius at P_o of 68 MPa and P_i of 6 MPa

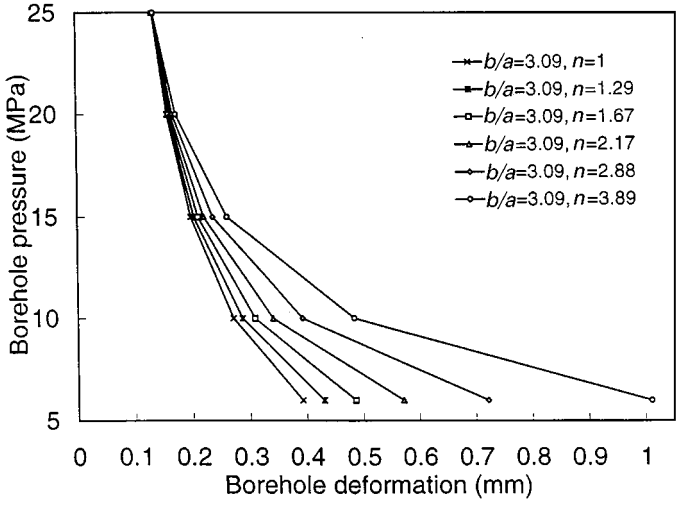

Figure 14. Comparison of borehole deformation under various non-associativity

(c) The borehole pressure should be decreased relatively fast so as to simulate the short-term behaviour of boreholes in the field. The borehole pressure reduction stage normally lasts 5–6 h.

The material properties and geometry used in the comparison are given in Table II (refer to Figure 1). The material properties were obtained from consolidated undrained triaxial tests (effective stress) on the synthetic shale.[20]

Table II. Material properties and geometry parameters

a (mm)	b (mm)	c (MPa)	ϕ (deg)	ψ (deg)	E (MPa)	ν	P_o (MPa)	K (m^3sec/kg)	P_i (MPa)	P_w (MPa)
12·8	39·6	6·3	36·2	0	20·38	0·32	68	$5{\cdot}14\times10^{-17}$	68 to 6	5

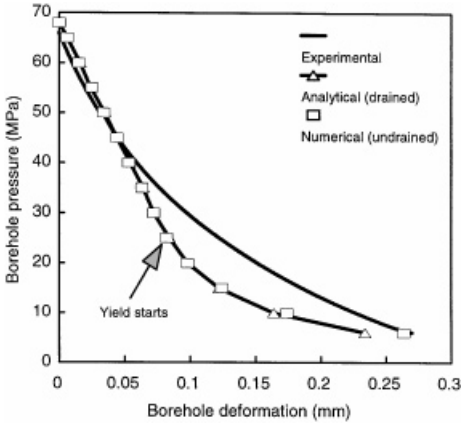

Figure 15. Borehole deformation versus borehole pressure of laboratory test, numerical modelling and derived analytical solution

The borehole deformation versus borehole pressure obtained from the laboratory test, numerical modelling and the analytical solution are presented in Figure 15. The figure shows a significantly non-linear deformation in the experimental results and as a result the onset of yielding cannot be determined accurately. As the linear elastic–perfect plasticity constitutive model is used in the numerical model and the analytical solution, similar results are obtained from the two methods. The elastic and plastic deformation stages can be clearly distinguished in the analytical and numerical results and hence, the initial yielding of the sample can be readily determined. As discussed in the previous section, both solutions predict onset of yielding at a borehole pressure of 27 MPa.

As previously stated, in the test, the borehole pressure was reduced to a minimum value of 6 MPa. As this pressure, the analytical and numerical models predict a yield zone of radius of 19·93 mm (see Section 3.2). If the borehole pressure is reduced to 0 MPa, a yield zone of radius of 30·86 mm is predicted. Although direct comparison with the thick-walled cylinder test is not possible, the fact that the sample did not fail during testing suggests that there is at least general agreement between the theoretical and experimental results.

In general, the predicted borehole deformations agree reasonably well with the experimental results. It shows that the linear elastoplastic constitutive model can give reasonable insights into the deformation and failure mechanisms of this shale. The adoption of a non-linear elastoplastic model may improve the agreement between experimental observation and numerical predictions. Such a model is currently being developed.

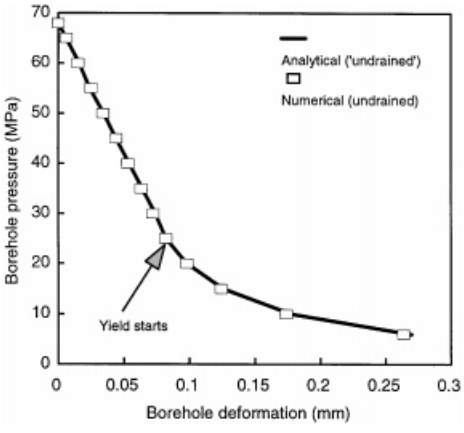

Figure 16. Borehole deformation versus borehole pressure of undrained numerical modelling and 'undrained' analytical solution

The increasing deviation between numerical model and analytical solution at the post-yield stage in Figure 15 is due to the difference in assumed drainage conditions. The numerical model is able to account for coupled flow and mechanical analysis under undrained conditions. In the other words, the pore pressure change in response to mechanical deformation is computed and flow is allowed under this condition. However, the analytical solution assumes fully drained conditions and therefore cannot account for pore pressure changes. Hence, the numerical model would be expected to give a better prediction than the analytical solution.

The comparison between experimental observation, numerical prediction and analytic solution shows that the analytical solution is adequate for situations in which there are no significant pore pressure changes. Although it is less accurate than numerical prediction for complex situations, its simplicity and easiness in use can provide a quick solution and hence, has a great advantage.

To further demonstrate the difference between numerical and analytical solutions due to drainage conditions, the constant pore pressures in the analytical model are replaced with the values obtained from the numerical model. This is referred to as an 'undrained' analytical solution (not truly undrained) since the pore pressure change has to be obtained by other means. Figure 16 shows the comparison of borehole deformations between the numerical modelling and 'undrained' analytical solution. It can be seen that the two predictions agree well with each other.

For stress environments and materials in which no significant pore pressure change occurs, the drained deformation from the analytical solution can be used with high accuracy. Conversely, pore pressure changes should be taken into account in using the analytical solution for the analysis of materials in which pore pressure changes will be significant.

5. CONCLUSIONS

In this paper, a closed-form solution is presented for the stress and displacement distributions in hollow cylinder subjected to uniform pressures acting on its internal and external boundary surfaces under plane strain conditions. Applications of the closed-form solution and comparison

with a previously published analytical solution, as well as a numerical model and experimental results are also presented. The following conclusions can be drawn from the study:

(1) The newly developed analytical solution has been verified with an infinite boundary closed-form solution, and a numerical analysis of a finite boundary borehole.
(2) The analytical solution can be used to calculate the stress and displacement distributions around a borehole and other cylindrical cavities under infinite and finite boundary conditions.
(3) The comparison of stress and displacement between the newly derived and infinite boundary solutions shows that an infinite boundary solution is a reasonable approximation if stresses are of concern. However, when determining stresses in material undergoing significant yield and/or accurate determination of displacement is important, the infinite boundary solution will lead to significant error.
(4) The dilation angle has a significant influence on deformation. Hence, a realistic dilation angle should be used for problems and applications where accurate deformation prediction is critical.
(5) The newly developed analytical solution has been compared with a laboratory collapse test on a thick-walled hollow cylinder, and shows a reasonably good agreement.
(6) The analytical solution is able to give reasonable insights into the deformation and failure mechanisms of wellbore and other axisymmetric problems in shale like materials.
(7) The analytical solution is flexible enough to be used to conduct undrained and drained analyses depending on the stress environment and the material investigated. For a stress environment and a material in which no significant pore pressure changes occur, the drained deformation obtained from the analytical solution can be used with high accuracy. Conversely, pore pressure change should be taken into account in using the analytical solution to analyse materials in which pore pressure changes are significant.

ACKNOWLEDGEMENTS

The authors would like to express their thanks to Dr. James Gunning (CSIRO Petroleum) for his help on the use of *Mathematica*™ in solving the closed-form equations and Dr. Bailin Wu (CSIRO Petroleum) for discussions on the experimental aspects of the borehole collapse test.

REFERENCES

1. B. Ladanyi, 'Expansion of cavities in brittle media', *Int. J. Rock Mech. Min. Sci.*, **4,** 301–328 (1967).
2. B. C. Haimson and T. M. Tharp, 'Stresses around boreholes in bilinear elastic rock', *6th SPE-AIME Conf. on Drilling and Rock Mechanics*, Austin, U.S.A., 1974, pp. 145–151.
3. A. L. Florence and L. E. Schwer, 'Axisymmetric compression of a Mohr–Coulomb medium around a circular hole', *Int. J. Numer. Analy. Meth. Geomech.*, **2,** 367–379 (1978).
4. P. Fritz, 'An analytical solution for axisymmetric tunnel problems in elasto-viscoplastic media', *Int. J. Numer. Anal. Meth. Geomech.*, **8,** 325–342 (1984).
5. J. P. Carter, J. R. Booker and S. K. Yeung, 'Cavity expansion in cohesive frictional soils', *Geotechnique*, **36,** 349–358 (1986).
6. I. D. R. Bradford and J. M. Cook, 'A semi-analytic elastoplastic model for wellbore stability with applications to sanding', SPE/ISRM *EUROCK'94: Rock Mechanics in Petroleum Engineering*, Delft, Netherlands, 1994, pp. 347–354.
7. A. Verruijt, 'A complex variable solution for a deforming circular tunnel in an elastic half-plane', *Int. J. Numer. Anal. Meth. Geomech.*, **21,** 77–89 (1997).
8. P. Papanastasiou and D. Durban, 'Elastoplastic analysis of cylindrical cavity problems in geomaterials', *Int. J. Numer. Anal. Meth. Geomech.*, **21,** 133–149 (1997).
9. R. Risnes, R. K. Bratli and Horsrud, P. 'Sand stresses around a wellbore', *SPE J.* **22,** 883–898 (1982).

10. M. Gumusoglu, Analysis of Underground Excavations in Strain Softening Rock Masses, *Ph.D. Thesis*, London University, 1986.
11. F. Santarelli and E. T. Brown, 'Performance of deep wellbores in rock with a confining pressure-dependent elastic modulus', *Proc. Int. Congress on Rock Mechanics*, Pau, France, Vol. 2, 1987, pp. 1217–1222.
12. D. R. Schmitt, R. J. Tait and H. Spann, 'Solution for pore pressure and stress in a porous hollow cylinder: application to a laboratory experiment', *Int. J. Rock Mech. Min. Sci.*, **30,** 1057–1060 (1993).
13. P. J. van den Hoek, G. M. M. Hertogh, A. P. Kooijman, Ph. de Bree, C. J. Kenter and Papamichos, 'A new concept of sand production prediction: Theory and laboratory experiments', *SPE Annual Technical Conf. and Exhibition 1996*, Denver, Colorado, U.S.A., 1996, pp. 19–33.
14. R. Hill, *The Mathematical Theory of Plasticity*, Oxford University Press, London, 1950.
15. Itasca Consulting Group, *FLAC User's Manual*, Minneapolis, Minnesota, U.S.A., 1995.
16. E. H. Davis, 'Theories of plasticity and the failure of soil masses', in I. K. Lee (ed.), *Soil Mechanics Selected Topics*, Butterworths, London, 1968, pp. 341–380.
17. X. Chen, C. P. Tan and C. M. Haberfield, 'Wellbore stability analysis guidelines for practical well design', *1996 SPE Asia Pacific Oil and Gas Conf.*, Adelaide, Australia, 1996, pp. 117–126.
18. S. P. Timoshenko and J. N. Coodier, *Theory of Elasticity*, 3rd edn., Tokyo, McGraw-Hill Kogakusha Ltd, 1970.
19. I. W. Johnston and S. K. Choi, 'A synthetic soft rock for laboratory model studies', *Geotechnique*, **36,** 251–263 (1986).
20. B. Wu and C.P. Tan, Consolidated undrained and drained triaxial tests of Johnstone, *APCRC Restricted Report*, No. 019, CSIRO Petroleum, Melbourne, Australia, 1996.

